

Impact Analysis of MPL on a PEFC Cell's Temperature Distribution with Thin PEM and GDL for Operating at Higher Temperature than Usual

Akira Nishimura¹, Nozomu Kono¹, Kyohei Toyoda¹, Yuya Kojima¹ and Mohan Lal Kolhe²

1. Division of Mechanical Engineering, Graduate School of Engineering, Mie University, Tsu-City, Mie 514-8507, Japan

2. Faculty of Engineering and Science, University of Agder, Kristiansand No. 4604, P.O. Box 422, Norway

Abstract: According to the New Energy and Industry Technology Development Organization (NEDO) road map 2017 of Japan, polymer electrolyte fuel cell (PEFC) system is required to be operated at 90 °C and 100 °C for stationary and mobility applications, respectively. However, the general PEFC, which has Nafion membrane is operated within the temperature range between 60 °C and 80 °C. It is important to understand the temperature distribution in a PEFC cell for analyzing performance on working life span of PEFC. This study focuses on the combination of thin polymer electrolyte membrane (PEM) and thin gas diffusion layer (GDL) to improve power generation performance under relatively higher temperature operation conditions. In addition, this study also focuses on effect of micro porous layer (MPL), which can promote the mass transfer, over temperature distribution. The key aim of this study is to analyze impact of MPL of temperature distribution on the reaction surface (T_{react}) of a cell of PEFC using thin PEM and GDL with variations of H_2 and O_2 supply flow rates and their relative humidity (RH) with changing the initial operating temperature (T_{ini}) from 80 °C to 100 °C. As a result, the distribution of T_{react} without MPL, for anode and cathode at 80 % RH and T_{ini} at 80 °C and 90 °C, is higher than normal conditions. There is a small difference in temperature distribution among different RH conditions with MPL. The distributions of T_{react} are relatively flat and almost the same among different RH conditions without MPL at $T_{\text{ini}} = 100$ °C, while the distributions of T_{react} with MPL are almost the same among different RH conditions. This study is revealed that more even temperature distribution and higher power generation performance can be obtained in the case without MPL compared to the case with MPL.

Key words: PEFC, temperature distribution analysis, MPL, thin PEM and thin GDL, higher temperature operation.

1. Introduction

It is an urgent requirement to decrease the CO_2 emissions in the world. Renewable energy can be used for H_2 production and can effectively contribute to solve the global warming problems through many applications. Polymer electrolyte fuel cell (PEFC) is an interesting combined heat and power generation technology, where H_2 is used as a fuel. According to New Energy and Industry Technology Development Organization (NEDO) road map 2017 of Japan [1], PEFC system is required to be operated at 90 °C and 100 °C for stationary and mobility applications,

respectively. However, the normal PEFC, which has Nafion membrane, is operated within the temperature range between 60 °C and 80 °C [2, 3]. If PEFC is operated at relatively higher temperature than usual, following advantages can be achieved: (1) promotion of electrochemical kinetics in both electrodes; (2) reducing the cooling system for automotive applications, because of increase in temperature difference between the PEFC stack and coolant; (3) endurance enhancement to CO which can be available on lower quality reformed H_2 [4]. However, we have to consider the following problems, if PEFC system is going to be operated at higher temperature: (1) degradation of polymer electrolyte membrane (PEM); (2) catalyst elution; (3) uneven distributions of gas flow, pressure, temperature, voltage and current in the

Corresponding author: Akira Nishimura, Ph.D., associate professor, research fields: heat transfer, fuel cell, photocatalyst and hydrogen production.

PEFC. They should be resolved to commercialize the PEFC system, which can be operated at higher temperature [5]. Moreover, the temperature distribution also influences the phase change of water and can influence the performance of PEM, fuel and oxidant flows in gas diffusion layer (GDL) and catalyst layer at high temperature. Therefore, it is important to analyze the temperature distribution in a cell of PEFC in order to improve the power generation performance and to achieve longer operational life span.

The characteristics of high temperature PEFC (HTPEFC) have been investigated recently for operating temperature over 100 °C [6-19]. However, most of them focused on development of new materials such as membrane and catalyst [6-12]. Some numerical studies [6-12] have reported analysis on distribution of current density, O₂ and water concentration under the condition changing assembly pressure [13]. The power generation performance has evaluated by polarization and power curves, when changing the thickness of membrane [14], electrolyte potential distribution evaluated by 2D and 3D model [15], and mathematical modeling to predict the degradation of membrane and catalyst [16]. The other experimental investigations have reported the effect of CrN/Cr coating stainless bipolar plate on the power generation performance improvement [17], the effect of flow rate and assembly pressure on the power generation performance using stainless bipolar plate [18], and the effect of gas pressure on the power generation performance [19]. A very few researchers [5, 20] have reported the investigation on temperature distribution in a cell of PEFC operated at relatively higher temperature. However, they did not investigate the temperature distribution near the interface between PEM and catalyst layer at the cathode, which has termed as a reaction surface in this study, except for the studies by the authors [21-23]. The previous research works by the authors [21-23] have investigated the impact of PEM's thickness as well as GDL's thickness on temperature distribution on the reaction surface (T_{react})

in a cell of PEFC at higher temperature such as 90 °C by the developed model using the temperature distribution data obtained by the thermograph experimentally. The impact of micro porous layer (MPL), which can improve not only the through-plane thermal conductivity of GDL [24] but also gas diffusion because of enhancement of discharging liquid water in catalyst layer [25], has been also investigated in this study. Through state-of-art literature review, it is observed that the impact of MPL on distribution of T_{react} in a cell of PEFC using thin PEM and GDL as well as initial operation temperature (T_{ini}) has not been investigated yet.

When we use thinner PEM, the lower Ohmic resistance as well as higher proton flux ratio and back diffusion [14, 26, 27] can be achieved. In addition, GDL's thickness influences O₂ concentration distribution in the catalyst layer and water discharge performance in the PEFC [28]. It is going to contribute to promoting the heat and mass transfer phenomena as well as the power generation performance of PEFC by decreasing the PEM and GDL's thickness. However, at present there is no study to clarify the distribution of T_{react} in a cell of PEFC using thin PEM and GDL at higher temperature such as 90 °C to 100 °C compared to usual operating temperature. This study considers that it is important to analyze the distribution of T_{react} , since the heat and water due to O₂ reduction reaction are generated. In addition, at present there is no study on investigating the impact of MPL on distribution of T_{react} in a cell of PEFC using thin PEM and GDL, when T_{ini} is changed from usual operating temperature to the higher temperature of 100 °C.

In this paper, the objective is to analyze the impact of MPL on distribution of T_{react} in a cell of PEFC using thin PEM and GDL with variations of flow rates and relative humidity (RH) of the supply gases for changing T_{ini} from usual operation temperature of 80 °C to higher temperature such as 90 °C and 100 °C. Additionally, this study is investigating the impact of MPL by comparing the results with and without MPL.

The present investigation is carried out using the heat transfer model developed by the authors [21-23].

The temperature distributions on separator's back of a cell of PEFC have been measured by thermograph and used in the heat transfer model [29]. Without disturbing the heat and mass transfer as well as power generation operation due to installation of sensor, the temperature distribution under loading conditions is measured accurately. Based on the measured data, the studies [23-25] have tried to build an empirical model to predict the distribution of T_{react} . Through the literature survey, it is observed that there has been no previous study on estimating the distribution of T_{react} from measured temperature data at the separator's back. The heat transfer model can predict the distribution of T_{react} with the measured separator's back temperature, and it is desirable to be developed. The distribution of T_{react} could be easily estimated without difficulty and complex temperature measurement using the presented heat transfer model.

In the previous studies conducted by authors [30-32], a 1D multi-plate heat transfer model using the temperature data of separator's back, has been measured by the thermograph under power generation. It has been used to estimate the temperature distribution in a cell of PEFC. A cell of PEFC consists

of PEM, catalyst layer, GDL and separator. The authors have proposed heat transfer model in Refs. [30-32], which has assumed the heat transfer through multi-plates for these cell components. The temperature at the interface between PEM and catalyst layer on the cathode, i.e., T_{react} is calculated using the heat transfer model [30-32]. This is a new approach to identify the heat transfer mechanism in a cell of PEFC by means of measured data by the thermograph and the developed model.

2. Analysis on Heat Transfer in Single Cell of PEFC

2.1 1D Multi-plate Heat Transfer Model

The multi-plate single cell PEFC module is illustrated in Fig. 1. In the module, the separator's back is opposite side of the surface contacting GDL. The separator's back is the opposite side of surface contacting GDL. The separator's back surface temperatures $T_{\text{surf},c}$ and $T_{\text{surf},a}$ are measured using the thermograph.

The heat transfer across the module is assumed to be in 1D direction only. In the module, the cell is divided into a gas channel and a rib part, and then the upper and lower parts represent rib part and channel part, respectively. For both parts, the heat transfer is assumed to be in the through-plane direction.

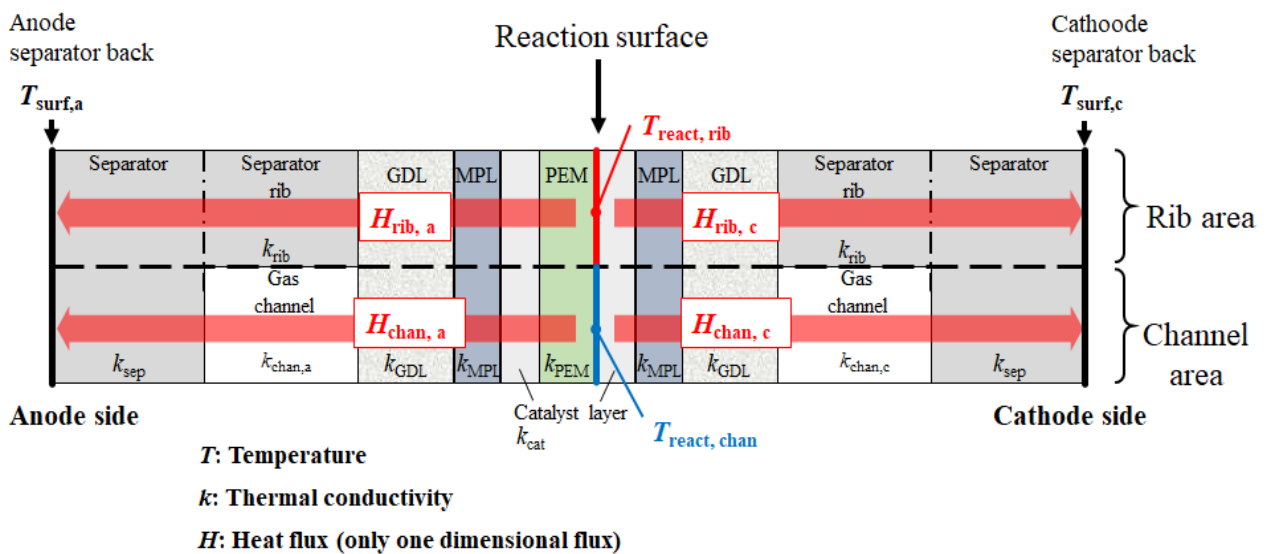


Fig. 1 1D multi-plate heat transfer module.

The heat generated on the reaction surface is transferred to the cathode and anode sides separately. Although the gas flowing through the gas channel from the inlet to the outlet of the cell carries away some heat, the amount of heat that is taken is less than 1% of the estimated reaction heat of approximately 20 W [31]. Therefore, the heat carried away by the gas flow is neglected in this model. Additionally, the mass flow rate of gas, flowing through the gas channel, is very small ranging from 10^{-8} to 10^{-6} kg/s, and it follows the assumption that the thermal conduction of gas in the gas channel is to be static.

2.2 Heat Generation Rate by Reaction in the Proposed Model

The heat generation rate H_{react} (as a reaction product), is calculated as:

$$H_{\text{react}} = E_i - W_E \quad (1)$$

where, E_i is the ideal (total) energy generation rate by the water formation from H_2 and O_2 based on the higher heating value (HHV). W_E is the electric power generated by PEFC. E_i and W_E are expressed as follows:

$$E_i = m_{H_2} \times q_{\text{HHV}} \quad (2)$$

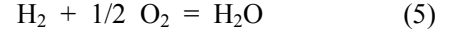
$$W_E = I \times V \quad (3)$$

where, I is the load current obtained by the experiment. The PEMs of Nafion 115, NRE-212 and NRE-211 are investigated in this study, I is kept at 20 A ($= 0.80 \text{ A/cm}^2$). V is the voltage obtained by the experiment. m_{H_2} is the molar flow rate of supplied H_2 , which is equal to the ideal reaction consumption rate of H_2 , required for the generation of 20 A, i.e., at the stoichiometric ratio (s.r.) of 1.0. Here, s.r. is the ratio of the feed amount of H_2 and O_2 required to generate a current of 20 A. The consumption rate of supply gas (H_2) at s.r. of 1.0 is defined as follow:

$$m_{H_2} = I/nF \quad (4)$$

where, m_{H_2} is the molar consumption rate of supplied H_2 at s.r. of 1.0 (mol/s), n is the valence ion ($= 2$ for H_2), F is the Faraday constant ($= 96,500 \text{ C/mol}$), m_{O_2} is the molar consumption rate of supplied O_2 at s.r. of

1.0 (mol/s) and it is calculated:



The actual s.r. of consumption rate of gas is confirmed, using the mass flow controller installed at the inlet of the single cell of PEFC, and the mass flow meter is installed at the outlet of the cell in the power generation experiment [29]. As a result, the consumption rates of supplied H_2 and O_2 are 1.0, respectively.

2.3 Heat-Balance Equations for Calculating Reaction Surface Temperature in the Proposed Model

The reaction heats at the rib and channel are expressed in Eqs. (6)-(10):

$$H_{\text{rib, c}} = K_{\text{rib, c}} A (T_{\text{react, rib}} - T_{\text{surf, c}})/2 \quad (6)$$

$$H_{\text{chan, c}} = K_{\text{chan, c}} A (T_{\text{react, chan}} - T_{\text{surf, c}})/2 \quad (7)$$

$$H_{\text{rib, a}} = K_{\text{rib, a}} A (T_{\text{react, rib}} - T_{\text{surf, a}})/2 \quad (8)$$

$$H_{\text{chan, a}} = K_{\text{chan, a}} A (T_{\text{react, chan}} - T_{\text{surf, a}})/2 \quad (9)$$

$$H_{\text{react}} = H_{\text{rib, c}} + H_{\text{chan, c}} + H_{\text{rib, a}} + H_{\text{chan, a}} \quad (10)$$

where, H is the heat flux (W), K is the overall heat transfer coefficient ($\text{W}/(\text{m}^2 \cdot \text{K})$), A is the heat transfer area which is the active area of MEA, i.e., power generation area ($= 0.0025 \text{ m}^2$), T is temperature (K or $^{\circ}\text{C}$). As to the subscripts, rib, chan, react, surf, c and a indicate under rib, under channel, reaction surface, separator's back surface, cathode side, anode side, respectively. $K_{\text{rib, c}}$, $K_{\text{rib, a}}$ and $K_{\text{chan, a}}$ are defined as follows:

$$1/K_{\text{rib, c}} = \delta_{\text{cat}}/k_{\text{cat}} + \delta_{\text{MPL}}/k_{\text{MPL}} + \delta_{\text{GDL}}/k_{\text{GDL}} + \delta_{\text{rib}}/k_{\text{rib}} + \delta_{\text{sep}}/k_{\text{sep}} \quad (11)$$

$$1/K_{\text{chan, c}} = \delta_{\text{cat}}/k_{\text{cat}} + \delta_{\text{MPL}}/k_{\text{MPL}} + \delta_{\text{GDL}}/k_{\text{GDL}} + \delta_{\text{chan}}/k_{\text{chan}} + \delta_{\text{sep}}/k_{\text{sep}} \quad (12)$$

$$1/K_{\text{rib, a}} = \delta_{\text{PEM}}/k_{\text{PEM}} + \delta_{\text{cat}}/k_{\text{cat}} + \delta_{\text{MPL}}/k_{\text{MPL}} + \delta_{\text{GDL}}/k_{\text{GDL}} + \delta_{\text{rib}}/k_{\text{rib, a}} + \delta_{\text{sep}}/k_{\text{sep}} \quad (13)$$

$$1/K_{\text{chan, a}} = \delta_{\text{PEM}}/k_{\text{PEM}} + \delta_{\text{cat}}/k_{\text{cat}} + \delta_{\text{MPL}}/k_{\text{MPL}} + \delta_{\text{GDL}}/k_{\text{GDL}} + \delta_{\text{chan}}/k_{\text{chan, a}} + \delta_{\text{sep}}/k_{\text{sep}} \quad (14)$$

where, δ_{cat} is thickness of the catalyst layer (m), k_{cat} is thermal conductivity of the catalyst layer ($\text{W}/(\text{m} \cdot \text{K})$), δ_{MPL} is thickness of MPL (m), k_{MPL} is thermal conductivity of MPL ($\text{W}/(\text{m} \cdot \text{K})$), δ_{GDL} is thickness of GDL (m), k_{GDL} is thermal conductivity of GDL

(W/(m·K)), δ_{rib} is thickness of the separator rib (m), k_{rib} is thermal conductivity of the separator rib (W/(m·K)), δ_{sep} is thickness of separator excluding rib part (m), k_{sep} is thermal conductivity of separator excluding rib part (W/(m·K)), δ_{chan} is thickness of the channel of separator (m), k_{chan} is thermal conductivity of the mixture gas in the channel of separator (W/(m·K)), δ_{PEM} is thickness of PEM (m), k_{PEM} is thermal conductivity of PEM (W/(m·K)).

The specification of cell components used in the proposed model is presented in Table 1. Nafion 115, NRE-212 and NRE-212 (manufactured by Do Pont Corp.), whose thicknesses are 127 μ m, 51 μ m and 25 μ m, respectively, are used and investigated in this study. In addition, TGP-H-060 and TGP-H-030 (manufactured by Toray Corp.) whose thicknesses are 190 μ m and 110 μ m, respectively, are investigated. The proposed model consists of PEM, catalyst layer, MPL, GDL and separator. The values of thickness, listed in Table 1, are same as those of the components used in the previous studies [23, 27, 29, 33, 34].

The effective thermal conductivities of porous media k are listed in Table 1. They are the values of cell components used in this experiment, and in the other references, too [27, 29]. In Table 1, the effective thermal conductivities are obtained when the cell

components pores are filled with air at room temperature. Therefore, the corrected effective thermal conductivities are calculated for the cell components pores filled with H₂ or O₂ at 80 °C, 90 °C and 100 °C, and they are representing T_{ini} in this study. In the power generation experiment whose data were used for the numerical analysis in this study [29], the single cell of PEFC was prepared by electric heater at T_{ini} before the temperature measurement by thermograph. In addition, the temperature of supply gas at the inlet is controlled by electric heater at T_{ini} . In the calculation, thermal conductivities of each supply gases are used from “The Japan Society of Mechanical Engineers” [35].

The temperatures are measured using the thermograph and substituted into the equations as $T_{surf, c}$ and $T_{surf, a}$ for solving Eqs. (6)-(9). Table 2 lists the operational conditions applied for PEFC power generation experiment to measure the temperatures with thermograph. 1D multi-plate heat transfer analysis used the data obtained under these experimental conditions. The current density is kept at 0.80 A/cm² in the PEFC power generation experiment in order to obtain the temperature data using thermograph. The temperature distribution data caused by the reaction heat at the separator back are obtained.

Table 1 Specification of PEFC components referred from the manufacture catalog and previous studies [23, 27, 29, 33].

Parts	Size	Characteristics	Porosity (-)	Effective thermal conductivity (W/(m·K))
Polymer electrolyte membrane (PEM)	50.0 mm × 50.0 mm × 0.127 mm (Nafion 115), 50.0 mm × 50.0 mm × 0.051 mm (NRE-212) or 50.0 mm × 50.0 mm × 0.025 mm (NRE-211)	Nafion 115, NRE-212 or NRE-211 (produced by Du Pont Corp.)	0.28	0.195
Catalyst layer	50.0 mm × 50.0 mm × 0.01 mm (attached with PEM)	Pt/C (20 wt% Pt loading)	0.78	0.27
Micro porous layer (MPL)	50.0 mm × 50.0 mm × 0.003 mm (attached with GDL)	Mixture of carbon black and PTFE	0.60	1.0
Gas diffusion layer (GDL)	50.0 mm × 50.0 mm × 0.19 mm (TGP-H-060) or 50.0 mm × 50.0 mm × 0.11 mm (TGP-H-030)	Carbon paper (TGP-H-060, TGP-H-030 produced by Toray Corp.)	0.78 (TGP-H-060)	1.7
Separator	75.4 mm × 75.4 mm × 2.00 mm (thickness of rib part: 1.00 mm) (Gas supply area: 50.0 mm × 50.0 mm)	Carbon graphite, serpentine	0.15	25

Table 2 Operating conditions of PEFC power generation for temperature measurement by thermograph.

Initial temperature of cell (T_{ini}) (°C)	80, 90, 100	
Load current of cell (A)	20 (0.80)	
(current density of cell ($A \cdot cm^{-2}$))		
Supply gas condition		
	Anode	Cathode
Gas type	H ₂	O ₂
Temperature of supply gas at inlet (°C)	80, 90, 100	80, 90, 100
Relative humidity of supply gas (% RH)	40, 80	40, 80
Pressure of supply gas at inlet (absolute) (MPa)	0.4	0.4
Flow rate of supply gas at inlet (NL·min ⁻¹) (stoichiometric ratio (-))	0.210 (1.5),	0.105 (1.5),
	0.280 (2.0),	0.140 (2.0),
	0.420 (3.0)	0.210 (3.0)

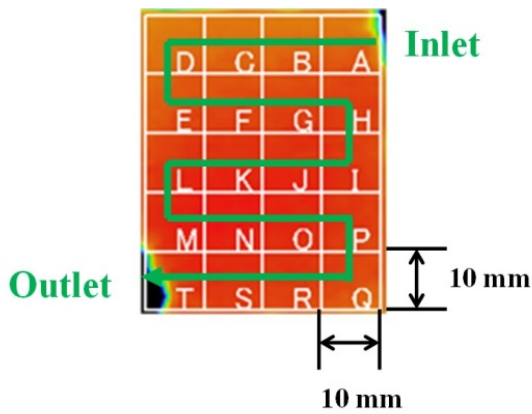


Fig. 2 Segment display of in-plane temperature distribution measured by thermograph.

The experimental procedure to measure the temperature during power generation has been explained in the authors' previous study [29].

As shown in Fig. 2, the in-plane temperature distribution is divided into the segments of 10 mm × 10 mm each in order to use the temperature data measured by the thermograph in 1D multi-plate in the heat transfer model. Though the power generation area is 50 mm × 50 mm, the observation area is set at 40 mm × 50 mm to prevent a gas leak through observation window in the experiments. The gas channel width and rib width at separator are 1.0 mm, and the number of gas channel is 5. Each segment consists of five parts of rib and gas channel. The average temperature in each segment at anode and cathode is considered for the separator's back temperature in 1D multi-plate heat transfer model. Fig. 2 illustrates the segments which are named from A to T along with the gas flow direction.

The insulators, covering the gas pipes, interfere with the thermograph measurement in some area of the segment (e.g. segments A and T) as it can be seen in Fig. 2. In this study, the effective temperatures of segments A and T are obtained by removing the temperature data that are interfered by the insulator from the total temperature data in each segment. In the heat transfer analysis, it is assumed that $T_{surf,c}$ on the rib side is equal to $T_{surf,c}$ on the cathode side as well as $T_{surf,a}$ since the difference between them could not be recognized by the measured data [21-23].

Considering the above described assumptions and Eqs. (6)-(14), the reaction surface temperature T_{react} is expressed as follows:

$$T_{react} = T_{react,rib} = T_{react,chan} = \{2H_{react}/A + (K_{rib,c} + K_{chan,c})T_{surf,c} + (K_{rib,a} + K_{chan,a})T_{surf,a}\} / (K_{rib,c} + K_{chan,c} + K_{rib,a} + K_{chan,a}) \quad (15)$$

where, T_{react} is calculated using H_{react} without estimating the local heat flux for each segment. Here, H_{react} is used to calculate T_{react} and it is used as a constant regardless of the segment. Additionally, i means the segment.

2.4 Model Validation

The model developed by the authors [30-32] has some difference, compared with the other heat transfer model [36-38] in terms of heat transfer conditions. However, the temperature gradients for the targeted regions, under the similar operational conditions, are almost the same [30]. In addition, the authors [39] have already investigated the 3D model using the

commercial CFD software to predict the distributions of T_{react} . This 3D model based on the described equations such as conservation equations of mass, momentum and energy in porous region as well as electrochemical reaction. Comparing the results of the 3D model with that of the 1D model proposed in this study under the several operation conditions, the differences of T_{react} between the two models were from 0.1 K to 1.5 K. Consequently, the 1D model proposed in this study has been validated by the 3D model. Thus, it can be considered that the proposed heat transfer model of this study is reasonable.

3. Results and Discussion

3.1 Impact of Flow Rate of Supply Gas at Inlet on Distribution of T_{react}

It is important to understand the impact of flow rates of supply gas at inlet on the heat and mass transfer phenomena as well as on power generation performance in order to manage the operational conditions for the actual operation usage. Fig. 3 shows the impact of stoichiometric ratio (s.r.) of supply gas at inlet on distribution of T_{react} simulated by the proposed heat transfer model with MPL. The RH of supply gas at inlet is 80% RH at anode and 80% RH at cathode (i.e., A80%RH, C80%RH). The s.r. of supply gas at inlet is 1.5, 2.0 and 3.0 $T_{\text{ini}} = 80\text{ }^{\circ}\text{C}$. The results are shown in Fig. 3.

According to Fig. 3, it is seen that the impact of flow rate of supply gas at inlet on the temperature distribution is not significant. The reason might be that the gas supply is sufficient for power generation at s.r. = 1.5 [22]. It is also established that the impact of flow rate of supply gas at the inlet on distribution of T_{react} is not significant irrespective of RH condition and T_{ini} as well as with and without MPL. According to the power generation experiments in this study [40], it indicates that the power generation performance is almost the same among different s.r. The results for s.r. = 1.5 are shown as the representative data in the following Sections 3.2 and 3.3.

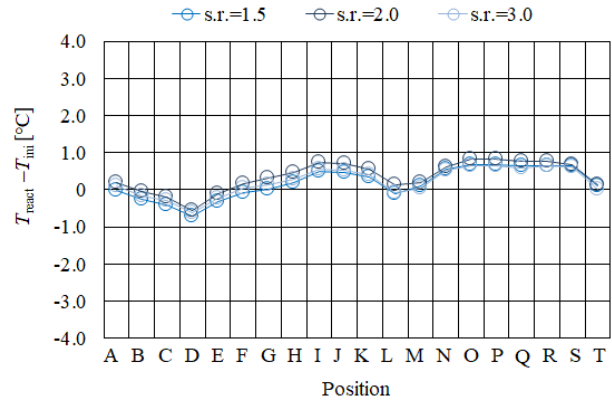


Fig. 3 Effect of stoichiometric ratio of supply gas on distribution of T_{react} ($T_{\text{ini}} = 80$; A80%RH, C80%RH; MPL W).

Additionally, it is observed from Fig. 3 that $T_{\text{react}} - T_{\text{ini}}$ drops at the position D, L and T. Regarding position L, it is believed that the water droplets are easy to remain since it is located at the corner of serpentine separator, the electrochemical reaction does not occur well. As a result, $T_{\text{react}} - T_{\text{ini}}$ drops in this position [32]. As to the position D, it is the inlet of the opposite side, i.e., anode side, resulting that the cell is cooled by the gas which is cooler than the cell heated by reaction heat [32]. On the other hand, as to the position T, water droplets are accumulated easily since the water with gas flow concentrates due to the outlet of the cell [21]. Therefore, the gas diffusion toward catalyst layer does not occur well, causing that the electro-chemical reaction is not followed well. As a result, $T_{\text{react}} - T_{\text{ini}}$ drops in this position.

3.2 Impact of PEM on Distribution of T_{react} When Using Thin PEM and Thin GDL

Figs. 4 and 5 show distributions of T_{react} changing RH conditions with and without MPL at $T_{\text{ini}} = 80\text{ }^{\circ}\text{C}$, respectively. According to Fig. 4, it is observed that the distributions of T_{react} without MPL for anode 80% RH and cathode 80% RH are higher than the other conditions. Since $T_{\text{ini}} = 80\text{ }^{\circ}\text{C}$ is usual operation temperature and anode 80% RH and cathode 80% RH are at well-humidified condition, it is thought that PEM is well hydrated along the gas flow from the inlet. On the other hand, it is observed from Fig. 4 that the

Impact Analysis of MPL on a PEFC Cell's Temperature Distribution with Thin PEM and GDL for Operating at Higher Temperature than Usual

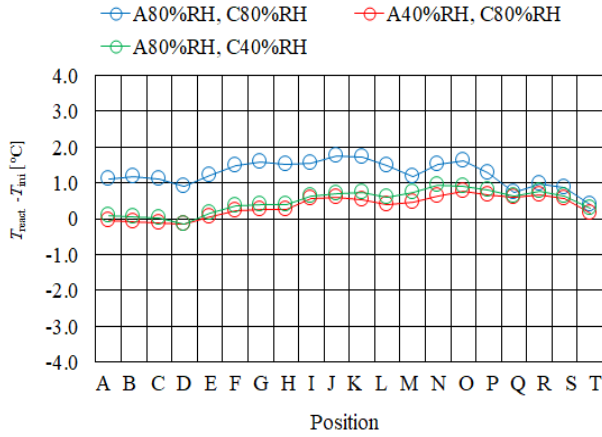


Fig. 4 Distribution of T_{react} changing RH conditions ($T_{\text{ini}} = 80$ °C; MPL W/O).

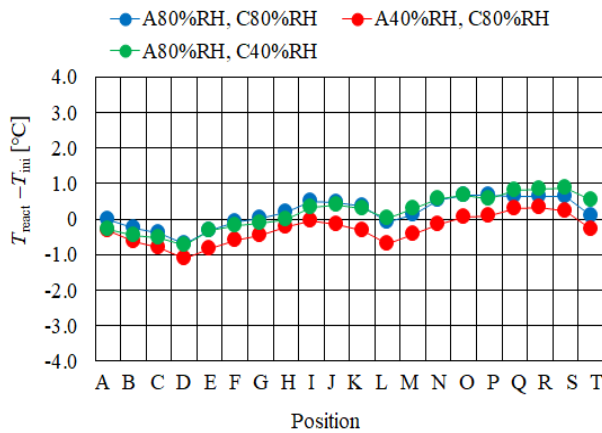


Fig. 5 Distribution of T_{react} changing RH conditions ($T_{\text{ini}} = 80$ °C; MPL W).

temperature increases along the gas flow from the inlet to the outlet by approximately 1 °C except for the above described condition. Since PEM is hydrated by the water produced by electrochemical reaction, the humidified gas flows through the gas channel. This trend indicates that the power generation is advanced along the gas flow [21, 22]. As a result, the temperature increases along the gas flow from the inlet to the outlet. Consequently, it is revealed that there is difference in the distributions of T_{react} among different RH conditions without MPL. According to Fig. 5, it is seen that the temperature increases along the gas flow from the inlet to the outlet by 1-2 °C irrespective of RH conditions. MPL has a role of discharging water to improve O_2 diffusion in catalyst layer [41], and promotion of back diffusion from cathode to anode by

the increase in the water vaporized due to increase in the temperature of catalyst layer at cathode [42]. MPL might support to discharge water, which is easy to be generated under well-humidified condition such as anode 80% RH and cathode 80% RH, resulting that the water transfer might be conducted from the inlet smoothly. Consequently, it is revealed that there is a small difference in temperature distribution among different RH conditions with MPL.

Distributions of T_{react} changing RH conditions with and without MPL at $T_{\text{ini}} = 90$ °C are shown in Figs. 6 and 7 respectively. According to Fig. 6, it is observed that the distribution of T_{react} without MPL for anode 80% RH and cathode 80% RH is higher than the other conditions, which has the same tendency as $T_{\text{ini}} = 80$ °C. Since anode 80% RH and cathode 80% RH is a well-humidified condition, it is thought that the PEM is well hydrated from the inlet even at high temperature of $T_{\text{ini}} = 90$ °C. On the other hand, it is observed from Fig. 6 that the temperature increases along the gas flow from the inlet to the outlet by approximately 1 °C except for the above described condition. Since PEM is hydrated by the water produced by electrochemical reaction and the humidified gas flows through the gas channel, it indicates that the power generation is progressed along the gas flow [21, 22]. As a result, the temperature increases along the gas flow from the inlet to the outlet. Consequently, it is revealed that there is difference in distributions of T_{react} among different RH conditions without MPL, which is the same as $T_{\text{ini}} = 80$ °C. According to Fig. 7, it is observed that the distribution of T_{react} with MPL for anode 80% RH and cathode 80% RH is higher than the other conditions, while the temperature increases along the gas flow from the inlet to the outlet by approximately 1.5-2 °C irrespective of RH conditions. MPL might support to discharge water which is easy to be generated under the well-humidified condition, such as anode 80% RH and cathode 80% RH, resulting that the water transfer is conducted from the inlet smoothly. However, the distribution of T_{react} with MPL for anode 80% RH and

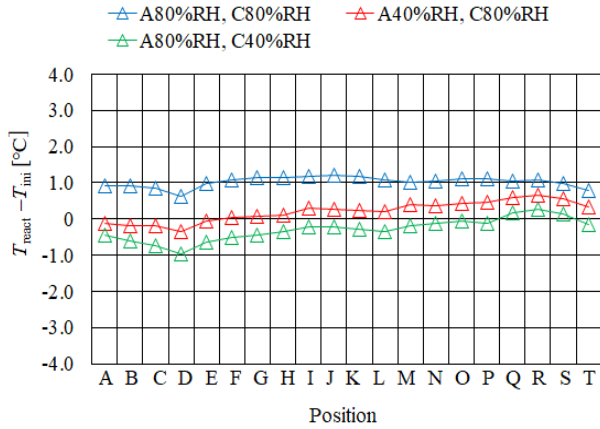


Fig. 6 Distribution of T_{react} changing RH conditions ($T_{\text{ini}} = 90\text{ }^{\circ}\text{C}$; MPL W/O).

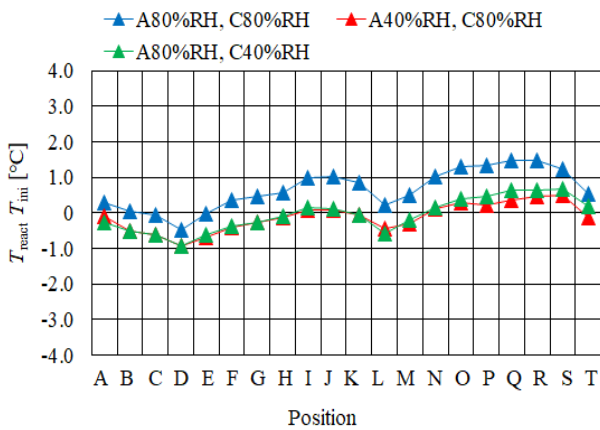


Fig. 7 Distribution of T_{react} changing RH conditions ($T_{\text{ini}} = 90\text{ }^{\circ}\text{C}$; MPL W).

cathode 80% RH is higher than the other conditions (Fig. 7). Since this study adopts thin PEM and thin GDL, we can obtain lower ohmic resistance, higher proton flux ratio of PEM [14, 26, 27] and reduction in mass transfer loss in GDL [28]. Therefore, the power generation performance is promoted, resulting in increasing the generated water as well as temperature with MPL for anode 80% RH and cathode 80% RH even at higher temperature of $T_{\text{ini}} = 90\text{ }^{\circ}\text{C}$.

Figs. 8 and 9 show distributions of T_{react} changing RH conditions with and without MPL at $T_{\text{ini}} = 100\text{ }^{\circ}\text{C}$, respectively. It is seen from Fig. 8 that distributions of T_{react} without MPL are relatively flat, i.e. whose variability is within $\pm 0.5\text{ }^{\circ}\text{C}$, though the temperature drop at the position D is observed. In addition, it is seen that distributions of T_{react} without MPL are almost the same among the different RH conditions. Since $T_{\text{ini}} =$

$100\text{ }^{\circ}\text{C}$ is higher temperature operation condition, PEM is easy to be dehydrated. Therefore, the power generation performance is declined due to reduction of H^+ conductivity [43]. In addition, it is believed that the impact of phase change of water as well as remaining the liquid water on gas diffusion in the cell is little at $T_{\text{ini}} = 100\text{ }^{\circ}\text{C}$ irrespective of RH conditions [44], resulting in uniform temperature distribution. According to Fig. 9, it is observed that distributions of T_{react} with MPL are almost the same among the different RH conditions. Since PEM is easy to be dehydrated at $T_{\text{ini}} = 100\text{ }^{\circ}\text{C}$ irrespective of RH condition, it is believed that the function of MPL discharging liquid water in catalyst layer [25] can not perform well. Therefore, distributions of T_{react} with MPL are almost the same among the different RH conditions.

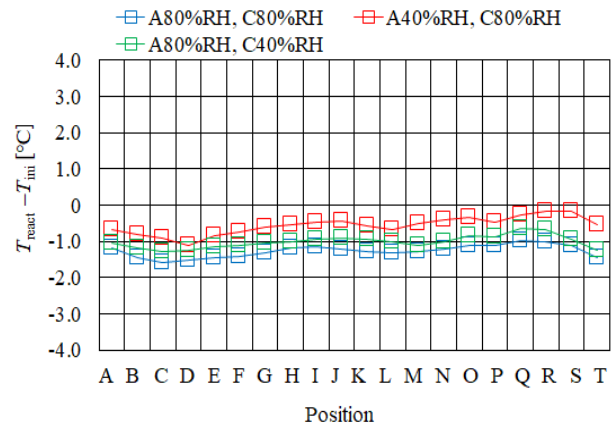


Fig. 8 Distribution of T_{react} changing RH conditions ($T_{\text{ini}} = 100\text{ }^{\circ}\text{C}$; MPL W/O).

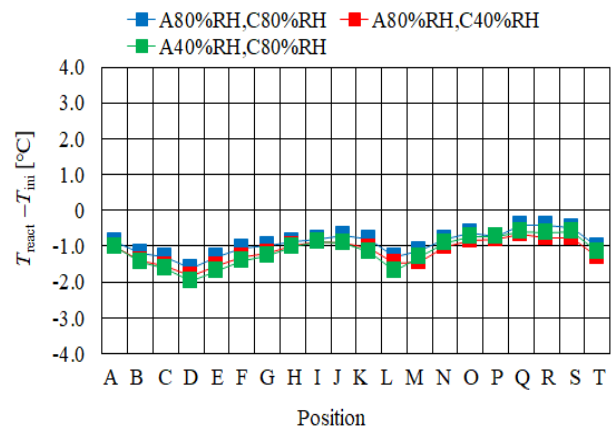


Fig. 9 Distribution of T_{react} changing RH conditions ($T_{\text{ini}} = 100\text{ }^{\circ}\text{C}$; MPL W).

Table 3 Comparison of power generation performance (unit: W).

T_{ini} (°C)	80		90		100	
	W	W/O	W	W/O	W	WO
A80%RH, C80%RH	11.3	11.5	10.9	12.0	8.37	9.63
A80%RH, C40%RH	10.7	11.6	10.5	11.6	8.28	9.63
A40%RH, C80%RH	10.8	11.6	10.6	12.0	7.83	9.54

3.3 Relationship between Temperature Distribution and Power Generation Performance

Table 3 lists the power obtained from the power generation experiment to measure $T_{surf, c}$ and $T_{surf, a}$ using thermograph. Load current is set at the constant value of 0.80 A/cm^2 during the power generation experiment. It is seen from Table 3 that the power decreases at $T_{ini} = 100 \text{ °C}$ for both cases with and without MPL, while the difference in power between $T_{ini} = 80 \text{ °C}$ and 90 °C is a small. PEM is easy to be dehydrated at $T_{ini} = 100 \text{ °C}$ since the water is vaporized. Therefore, the power generation performance is declined. Additionally, it is observed from Table 3 that the difference in power is small among different RH conditions for both cases with and without MPL. Using thin PEM and GDL provides the enhancement of water transfer between both electrodes, especially under lower RH condition at one side, resulting in improvement of water transfer from high RH side to low RH side. As a result, it is thought that the power generation performance under low RH condition at one side can obtain the same level as that under well humidified condition such as the anode 80% RH and cathode 80% RH (A80%RH, C80%RH). Moreover, it is revealed from Table 3 that the power with MPL is lower than that without MPL irrespective of T_{ini} . MPL can support to prevent flooding by discharging the liquid water from catalyst layer to GDL at medium temperature such as 60 °C [25]. The higher operation temperature conditions can dry up PEM, resulting that the function of MPL which promotes to discharge the liquid water from catalyst layer might bring the negative effect. Consequently, it is observed that the power with MPL is lower than that without MPL.

Considering the relationship between temperature distribution and power generation performance, the more even temperature distribution and higher power generation performance are obtained in the case without MPL, compared to the case with MPL. Since this study adopts the combination of thin PEM and thin GDL, we can obtain lower ohmic resistance, higher proton flux ratio of PEM [14, 26, 27] and reduction in mass transfer loss in GDL [28]. We can also obtain the enhancement of water transfer between both electrodes, when using the combination of thin PEM and thin GDL, which eliminates the use of MPL. Consequently, this study proposes using the combination of thin PEM and thin GDL without MPL for higher temperature operation.

4. Conclusions

This study has analyzed and investigated the temperature distribution on reaction surface by the 1D multi-plate heat transfer model by changing the flow rate (s) and RH of supply gas at the inlet as well as T_{ini} with and without MPL. The experimental results are used for the analysis. From the investigation, the following conclusions are drawn.

The impact of flow rate of supply gas at the inlet on the distribution of T_{react} is not significant irrespective of RH condition and T_{ini} as well as with and without MPL.

At $T_{ini} = 80 \text{ °C}$ and 90 °C , the distribution of T_{react} without MPL for anode 80% RH and cathode 80% RH is higher than the other conditions, while there is a small difference in the distribution of T_{react} among different RH conditions with MPL.

At $T_{ini} = 100 \text{ °C}$, the distributions of T_{react} are relatively flat, i.e. whose variability is within $\pm 0.5 \text{ °C}$

and almost the same among the different RH conditions without MPL. In addition, the distributions of T_{react} with MPL are almost the same among the different RH conditions.

The more even temperature distribution and higher power generation performance are obtained in case without MPL compared to case with MPL. It provides a relationship between temperature distribution and power generation performance.

It can be proposed that combination of thin PEM and thin GDL without MPL is desirable for more power generation under relatively higher temperature operation condition than usual.

Acknowledgments

This work is supported by Mie Prefecture Industrial Research Institute and the authors gratefully acknowledge.

References

- [1] NEDO (New Energy and Industry Technology Development Organization). "Technology Development Roadmap (Household Fuel Cell). <http://www.nedo.go.jp/content/100871973.pdf>.
- [2] Zhang, G., and Kandlikar, S. G. 2012. "A Critical Review of Cooling Technique in Proton Exchange Membrane Fuel Cell Stacks." *International Journal of Hydrogen Energy* 37 (Feb.): 2412-29.
- [3] Agbossou, K., Kolhe, M., Hamelin, J., and Bose, T. K. 2004. "Performance of a Stand-Alone Renewable Energy System Based on Energy Storage as Hydrogen." *IEEE Transactions on Energy Conversion* 19 (Oct.): 633-40.
- [4] Li, Q., He, R., Jensen, J. O., and Bjerrum, N. J. 2003. "Approaches and Recent Development Polymer Electrolyte Membrane for Fuel Cells Operating above 100 °C." *Chemical of Materials* 15 (26): 4896-915.
- [5] Lee, C. Y., Wang, F., Kuo, Y. W., Tsai, C. H., Cheng, Y. T., Cheng, C. K., and Lin, J. T. 2016. "In-Situ Measurement of High-Temperature Proton Exchange Membrane Fuel Cell Stack Using Flexible Five-in-One Micro-sensor." *Sensors* 16. doi: 10.3390/s16101731.
- [6] Budak, Y., and Devrim, Y. 2020. "Micro-cogeneration Application of a High-Temperature PEM Fuel Cell Stack Operated with Polybenzimidazole Based Membranes." *International Journal of Hydrogen Energy* 45: 35198-207.
- [7] Kim, D. H., Min, C. M., Lee, E., Lee, J. S., and Pak, C. 2020. "Effect of Vinylphosphonic Acid and Polymer Binders with Phosphate Groups on Performance of High-Temperature Polymer Electrolyte Membrane Fuel Cell." *Catalysis Today* 358: 333-7.
- [8] Lee, W., Lee, J. S., Park, H. Y., Park, H. S., Lee, S. Y., Song, K. H., and Kim, H. J. 2020. "Improvement of Fuel Cell Performance through the Enhanced Dispersion of the PTFE Binder in Electrodes for Use in High Temperature Polymer Electrolyte Membrane Fuel Cells." *International Journal of Hydrogen Energy* 45: 32825-33.
- [9] Sasiwimonrit, K., and Chang, W. C. 2020. "To Improve the High Temperature Polymer Electrolyte Membrane Fuel Cells Performance by Altering the Properties of Catalyst Layer." *International Journal of Hydrogen Energy* 45: 14491-9.
- [10] Wang, D., Wang, S., Tina, X., Li, J., Liu, F., Wang, X., Chen, H., Mao, T., and Liu, G. 2020. "Ethyl Phosphoric Acid Grafted Amino-Modified Polybenzimidazole with Improved Long-Term Stability for High-Temperature Proton Exchange Membrane Applications." *International Journal of Hydrogen Energy* 45: 3176-85.
- [11] Kannan, A., Kaczeriwski, J., Kabza, A., and Sholta, J. 2018. "Operation Strategies Based on Carbon Corrosion and Lifetime Investigations for High Temperature Polymer Electrolyte Membrane Fuel Cell Stacks." *Fuel Cells* 3: 287-98.
- [12] Quartarone, E., Angioni, S., and Mustarelli, P. 2017. "Polymer and Composite Membranes for Proton-Conducting, High-Temperature Fuel Cells: A Critical Review." *Materials* 10 (687): 1-17.
- [13] Zhang, T., Li, J., Li, Q., Yu, M., and Sun, H. 2021. "Combination Effects of Flow Field Structure and Assembly Force on Performance of High Temperature Proton Exchange Membrane Fuel Cells." *International Journal of Energy Research*. doi: 10.1002/er.6374.
- [14] Zhu, G., Chen, W., Lu, S., and Chen, X. 2019. "Parameter Study of High-Temperature Proton Exchange Membrane Fuel Cell Using Data-Driven Models." *International Journal of Hydrogen Energy* 44: 28958-67.
- [15] Lakshmi, B., Harikrishnan, N. P., and Juliet, A. V. 2017. "Comparative Analysis of 2D and 3D Model of a PEMFC in COMSOL." *Applied Surface Science* 418: 99-102.
- [16] Rasheed, R. K. A., Liao, Q., Caizhi, Z., and Chan, S. H. 2017. "A Review on Modeling of High Temperature Proton Exchange Membrane Fuel Cells (HT-PEMFCs)." *International Journal of Hydrogen Energy* 42: 3142-65.
- [17] Li, R., Cai, Y., Wippermann, K., and Lehnert, W. 2019. "Bilayer CrN/Cr Coating-Modified 316L Stainless Steel Bipolar Plates for High Temperature Polymer Electrolyte Fuel Cells." *Journal of Power Sources* 434: doi: 10.1016/j.jpowsour.2019.226718.
- [18] Chen, C. Y., and Su, S. C. 2018. "Development and Performance Evaluation of a High Temperature Proton

- Exchange Membrane Fuel Cell with Stamped 304 Stainless Steel Bipolar Plates.” *International Journal of Hydrogen Energy* 4: 13430-9.
- [19] Akimoto, F., Sasabe, T., Yoshida, T., Naito, H., Kawamura, K., and Hirai, S. 2019. “Investigation of Effects of High Temperature and Pressure on Polymer Electrolyte Fuel Cell with Polarization Analysis and X-Ray Imaging of Liquid Water.” *Journal of Power Sources* 431: 205-9.
- [20] Rasheed, R. K. A., and Chan, S. H. 2016. “Analysis of Steady State Heating Configuration for High-Temperature Proton Exchange Membrane Fuel Cell Based on Multi-physical Numerical Modeling.” *Electrochimica Acta* 222: 280-92.
- [21] Nishimura, A., Yamamoto, K., Okado, T., Kojima, Y., Hirota, M., and Kolhe, M. L. 2020. “Impact of Analysis of MPL and PEM Thickness on Temperature Distribution within PEFC Operating at Relatively Higher Temperature.” *Energy* 205: 117875. doi: 10.1016/j.energy.2020.117875.
- [22] Nishimura, A., Sato, Y., Kamiya, S., Okado, T., Yamamoto, K., Hirota, M., and Hu, E. 2019. “Impact of Thickness of Polymer Electrolyte Membrane and Gas Diffusion Layer on Temperature Distributions in Polymer Electrolyte Fuel Cell Operated at Temperature Around 90 °C.” *J. Energy Power Eng.* 13: 97-115.
- [23] Nishimura, A., Sato, Y., Yoshimura, M., Kamiya, S., and Hirota, M. 2018. “Impact of Thickness of Polymer Electrolyte Membrane on Temperature Distribution in Single Cell of Polymer Electrolyte Fuel Cell Operated at High Temperature.” *Journal of Energy and Power Engineering* 12: 80-92.
- [24] Zamel, N., Becker, J., and Wiegmann, A. 2012. “Estimating the Thermal Conductivity and Diffusion Coefficient of the Microporous Layer of Polymer Electrolyte Membrane Fuel Cells.” *Journal of Power Sources* 207: 70-80.
- [25] Chen, G., Zhang, G., Guo, L., and Liu, H. 2016. “Systematic Study on the Functions and Mechanisms of Micro Porous Layer on Water Transport in Proton Exchange Membrane Fuel Cells.” *International Journal of Hydrogen Energy* 41: 5063-73.
- [26] Springer, T. E., Zawadzinski, T. A., and Gottesfeld, D. 1991. “Polymer Electrolyte Fuel Cell Models.” *Journal of Electrochemical Society* 138: 2334-41.
- [27] Penga, Z., Tolj, I., and Barbir, F. 2016. “Computational Fluid Dynamics Study of PEM Fuel Cell Performance for Isothermal and Non-uniform Temperature Boundary Conditions.” *International Journal of Hydrogen Energy* 41: 17585-94.
- [28] Epting, W. K., and Lister, S. 2016. “Microscale Measurements of Oxygen Concentration across the Thickness of Diffusion Media in Operating Polymer Electrolyte Fuel Cells.” *Journal of Power Sources* 44: 674-86.
- [29] Nishimura, A., Shibuya, K., Morimoto, A., Tanaka, S., Hirota, M., Nakamura, Y., Kojima, M., Narita, M., and Hu, E. 2012. “Dominant Factor and Mechanism of Coupling Phenomena in Single Cell of Polymer Electrolyte Fuel Cell.” *Applied Energy* 90 (1): 73-9.
- [30] Nishimura, A., Iio, K., Baba, M., Yamauchi, T., Hirota, M., and Hu, E. 2014. “Modeling of Heat Transfer in Single Cell of Polymer Electrolyte Fuel Cell by Means of Temperature Data Measured by Thermograph.” *Journal of Chemical Engineering of Japan* 47 (7): 521-9.
- [31] Nishimura, A., Fukuoka, T., Baba, M., Hirota, M., and Hu, E. 2015. “Clarification on Temperature Distribution in Single Cell of Polymer Electrolyte Fuel Cell under Different Operation Conditions by Means of 1D Multi-plate Heat-Transfer Model.” *Journal of Chemical Engineering of Japan* 48 (10): 862-71.
- [32] Nishimura, A., Osada, K., Tsunoda, T., Yoshimura, M., Hirota, M., and Hu, E. 2016. “Analysis on Temperature Distributions in Single Cell of Polymer Electrolyte Fuel Cell When Operated in High Temperature Range.” *Journal of Energy and Power Engineering* 10: 453-64.
- [33] Cooper, N. J., Santamaria, A. D., Becton, M. K., and Park, J. W. 2017. “Neutron Radiography Measurements of *In-Situ* PEMFC Liquid Water Saturation in 2D & 3D Morphology Gas Diffusion Layers.” *International Journal of Hydrogen Energy* 42: 16269-78.
- [34] Kang, K., and Ju, H. 2009. “Numerical Modeling and Analysis of Micro-porous Layer Effects in Polymer Electrolyte Fuel Cells.” *Journal of Power Sources* 194: 763-73.
- [35] The Japan Society of Mechanical Engineers. 1993. *JSME Heat Transfer Handbook*. Tokyo: Maruzen.
- [36] Khandelwal, M., and Mench, M. M. 2006. “Direct Measurement of Through-Plane Thermal Conductivity and Contact Resistance in Fuel Cell Materials.” *Journal of Power Sources* 161 (2): 1106-15.
- [37] Kawase, M., Inagaki, T., Kawashima, S., and Miura, K. 2009. “Effective Thermal Conductivity of Gas Diffusion Layer in Through-Plane Direction.” *ECS Transactions* 25 (1): 1529-37.
- [38] Jung, C. Y., Shim, H. S., Koo, S. M., Lee, S. H., and Yi, S. C. 2012. “Investigation of the Temperature Distribution in Proton Exchange Membrane Fuel Cell.” *Applied Energy* 93 (May): 733-41.
- [39] Nishimura, A., Zamami, K. P., Yoshimoto, M., Hirota, M., and Kolhe, M. L. 2017. “Numerical Analysis of Temperature Distributions in Single Cell of Polymer Electrolyte Fuel Cell When Operated in Elevated

- Temperature Range.” *Journal of Energy and Power Engineering* 11: 393-408.
- [40] Nishimura, A., Okado, T., Kojima, Y., Hirota, M., Hu, E. 2020. “Impact of MPL on Temperature Distribution in Single Polymer Electrolyte Fuel Cell with Various Thickness of Polymer Electrolyte Membrane.” *Energies* 13. doi: 10.3390/en13102499.
- [41] Blanco, M., and Wilkinson, D. P. 2014. “Investigation of the Effect of Microporous Layers on Water Management in a Proton Exchange Membrane Fuel Cell Using Novel Diagnostic Methods.” *International Journal of Hydrogen Energy* 39: 16390-404.
- [42] Zhou, J., Shukla, S., Putz, A., and Secanell, M. 2018. “Analysis of the Role of the Microporous Layer in Improving Polymer Electrolyte Fuel Cell Performance.” *Electrochimica Acta* 268: 366-82.
- [43] Yang, C., Srinivasan, S., Bocarsly, A. B., Tulyani, S., and Benziger, J. B. 2004. “Comparison of Physical Properties and Fuel Cell Performance of Nafion and Zirconium Phosphate/Nafion Composite Membranes.” *J. Membrane Science* 237: 145-61.
- [44] Nishimura, A., Mahadi, A. H., Osada, K., Baba, M., and Hirota, M. 2015. “Heat and Mass Transfer Characteristics on Single-Cell of Polymer Electrolyte Fuel Cell Operated at Higher Temperature Than Usual.” *Kagaku Kogaku Ronbunshu* 41: 397-405.